

# Efficient Spintronic THz Emitters Without External Magnetic Field

Amir Khan,<sup>1</sup> Nicolas Sylvester Beermann,<sup>2</sup> Shalini Sharma,<sup>1</sup> Tiago de Oliveira Schneider,<sup>1</sup> Wentao Zhang,<sup>2</sup> Dmitry Turchinovich,<sup>2</sup> and Markus Meinert<sup>1</sup>

<sup>1</sup>*New Materials Electronics Group, Technical University of Darmstadt, Merckstr. 25, 64283 Darmstadt, Germany*

<sup>2</sup>*Faculty of Physics, Bielefeld University, Universitätsstraße 25, 33615 Bielefeld, Germany*

(\*Electronic mail: markus.meinert@tu-darmstadt.de)

(\*Electronic mail: amir.khan@tu-darmstadt.de)

(Dated: 8 November 2024)

We investigate the performance of state-of-the-art spintronic THz emitters (W or Ta)/CoFeB/Pt with non-magnetic underlayer deposited using oblique angle deposition. The THz emission amplitude in the presence or absence of an external magnetic field remains the same and remarkably stable over time. This stability is attributed to the enhanced uniaxial magnetic anisotropy in the ferromagnetic layer, achieved by oblique angle deposition of the underlying non-magnetic layer. Our findings could be used for the development of practical field-free emitters of linearly polarized THz radiation, potentially enabling novel applications in future THz technologies.

The spin of the electrons in conjunction with their charge has recently<sup>1</sup> paved the way to generating the terahertz (THz) radiation that covers the range of 0.1-30 THz using the devices called spintronic THz emitters (STEs). These are heterostructures of ferromagnetic (FM)/non-magnetic (NM) thin films with the magnetization in the film plane. The total metal thicknesses are ideally around 4 to 6 nanometers<sup>2</sup>. An ultrashort laser pulse excites the electrons and drives a spin current from the FM layer to the NM layer(s), which is converted into an in-plane charge current via the inverse spin Hall effect (ISHE)<sup>3,4</sup> in the NM layer(s). This short charge current burst then radiates a single cycle THz pulse<sup>5</sup>. The amplitude and polarization of the THz wave are independent of both the pump wavelength and polarization<sup>1,6</sup>. Notably, this process is also responsible for the demagnetization of the FM layer in femtosecond timescale (ultrafast laser-driven demagnetization<sup>7</sup>).

The STEs<sup>2,5</sup> produce THz waves with amplitude comparable to, or even higher than other types of tabletop THz emitters (electro-optic crystals, semiconductor antennas, and air plasma induced by femtosecond laser beam are among the standard methods for producing tabletop THz emitters). Importantly, the efficiency and polarization of THz waves from STEs depends on the magnetization of the FM layer which can be controlled by applying an external magnetic field<sup>8,9</sup>. However, this reliance on a constant external magnetic field for magnetic saturation of the FM layer for the THz emission limits STEs applications in environments where such fields are undesirable and also impede in downsizing the STEs for spintronic devices. To address this limitation, research on magnetic-field-free STEs is ongoing and holds promise for the next generation of THz technologies. Eliminating the need for external static fields in coherent terahertz emission may open the path for compact, field-free terahertz sources with applications such as THz magneto-optical spectroscopy for field sensitive materials<sup>10,11</sup>.

THz emission from the spintronic structures without external magnetic field has been previously reported<sup>1,12</sup>. However, more than 50% reduction in the THz emission amplitude was observed in comparison to the emission in the

presence of the external magnetic field. More recently it has been reported that in-plane uniaxial magnetic anisotropy (UMA) in the ferromagnetic layer can be utilized for field-free STEs<sup>13,14</sup>. These reports proposed a method of oblique angle deposition (OAD) of ferromagnetic layer in CoFeB/Pt bilayer structure and enhancement in UMA by varying the growth conditions of the single CoFeB layer, such as rotating it during the growth process. However, anisotropy through oblique deposition of the FM layer has limitations in achieving sufficiently high in-plane UMA, as in this case one is limited to very thin films. Further, the UMA can be deteriorated by annealing due to microstructural modifications or stress relaxation<sup>15,16</sup>. The enhancement in the in-plane UMA induced through oblique deposition of the NM underlayer has been previously explained by the formation of a ripple surface<sup>17-19</sup>, where the easy axis orientation depends on the details of the ripple structure. Notably, higher UMA leads to high stability against external field disturbances and enables longer-duration field-free STEs, and such STEs could be used for practical field-free THz spintronic emitters. STEs utilizing antiferromagnetic (AFM) materials to achieve field-free THz emission were recently reported<sup>20,21</sup> with AFM/FM/NM heterostructures. However, the growth of this type of heterostructures, as well as maintaining a robust exchange bias at the AFM/FM interface are difficult to achieve. This exchange bias arises from the interfacial interaction between the AFM and FM layers, significantly influencing the magnetic properties of the FM layer. However, at room temperature, the formation of a robust exchange bias at the AFM/FM interface presents a significant challenge given by the very thin metallic layers required for efficient THz emission. This limitation is further aggravated by elevated temperatures during the laser-excitation, posing an obstacle to the practical application of AFM-based field-free STEs. Oblique-angle-deposited STEs with enhanced UMA offer a simpler way for field-free THz spintronic emitters.

In this letter, we demonstrate a method to establish in-plane UMA for external magnetic field-free STEs. We introduce ripple structures (through self-shadowing<sup>22</sup> and steering effects<sup>23</sup>) by obliquely depositing the NM underlayer (W or

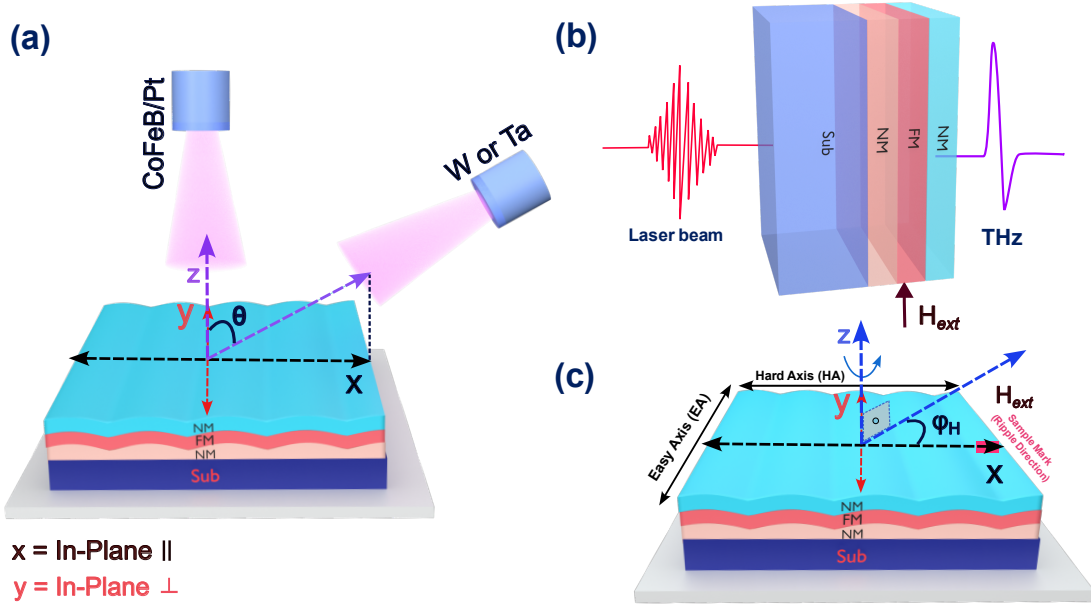


FIG. 1. Spintronic THz emitters deposition and measurement geometry. (a) W or Ta seed layer deposited at  $\theta = 0^\circ, 30^\circ$  and  $60^\circ$ . (b) A typical NM/FM/NM STEs geometry. (c) The THz emission measurement geometry: The sample is placed in the x-y plane with the laser beam propagating along the z-axis and  $\phi_H$  denotes the azimuthal angle between sample mark and in-plane applied external magnetic field, where the sample mark represents incoming material flux direction or ripple direction for obliquely deposited NM underlayer.

Ta) instead of the FM layer. We have achieved the external magnetic field-free THz emission from such structures, where the THz emission amplitude remains nearly the same after removing the applied external magnetic field.

We employed the NM 2 nm / Co<sub>40</sub>Fe<sub>40</sub>B<sub>20</sub> 2 nm / Pt 2 nm (where NM = W or Ta) STEs design known for its high-field THz emission<sup>2</sup>. These trilayer structures were deposited with a custom magnetron co-sputtering system with eight 2" sources by Bestec GmbH, Berlin. The target-to-substrate distance was approximately 12 cm, and the angle of incidence with respect to the sample stage normal was  $30^\circ$ . The base pressure was lower than  $5 \times 10^{-8}$  mbar, and the working gas pressure was  $2 \times 10^{-3}$  mbar at room temperature. The films were prepared by dc sputtering on double-side polished fused silica substrates with growth rates at  $30^\circ$  incidence angle of 0.116 nm/s (Ta), 0.064 nm/s (W), 0.039 nm/s (CFB), and 0.111 nm/s (Pt), respectively. No external magnetic field was applied during growth, and no post-annealing was performed. To achieve homogeneous, isotropic samples, the sample stage can be rotated with up to 30 rpm. In our growth process, the NM underlayers were deposited by varying  $\theta$  angles (see Fig. 1(a)) using the standard sample stage, or by equipping it with an additional  $30^\circ$  wedge-shaped holder and aligning it facing the source or away from the source. In all cases, the NM layer was deposited without rotation. This results in three different deposition modes which are summarized in Table I.

We have deposited two series of trilayer spintronic structures with either Ta or W as the NM underlayer, where the sample names will be referred to as the name of the under-

TABLE I. Deposition modes of NM (= W or Ta) underlayer

Sample Names	NM at angle ( $\theta$ )	FM/Pt at angle ( $\theta$ )	Rotation (rpm)
W30° or Ta30°	$30^\circ$	$30^\circ$	(FM/Pt) 20
W0° or Ta0°	$0^\circ$	$0^\circ$	0
W60° or Ta60°	$60^\circ$	$0^\circ$	0

layer followed by the deposition angle ( $\theta$ ), as summarized in Table I. We measured the thickness of the layers using X-ray reflectivity (XRR) with a Rigaku SmartLab (9 kW rotating anode) system. The deposition times were adjusted to match the 2 nm layer thickness for every single layer.

The in-plane UMA was investigated using the longitudinal magneto-optical Kerr effect (L-MOKE) with applied in-plane magnetic fields parallel and perpendicular to the ripple direction. The results are shown in Fig. 2, with the anisotropy increases with increasing angle  $\theta$ . Samples with oblique deposition show UMA with hard axis (HA) parallel to the plane of incident material flux direction or ripple direction and easy axis (EA) perpendicular to the plane of incident material flux direction or ripple direction. The samples were marked along ripple direction for reference, shown in Fig. 1 (c). In particular, we obtain a large anisotropy field with  $\mu_0 H_a \approx 44$  mT for  $\theta = 60^\circ$ , see Fig. 2(e) and (f). This corresponds to a uniaxial anisotropy constant of  $K_u = \mu_0 H_a M_s / 2 \approx 21.8$  kJ/m<sup>3</sup> with the saturation magnetization  $M_s = 990$  kA/m, as determined by broadband ferromagnetic resonance spectroscopy up to 30 GHz on an isotropic CFB film of 5 nm thickness.

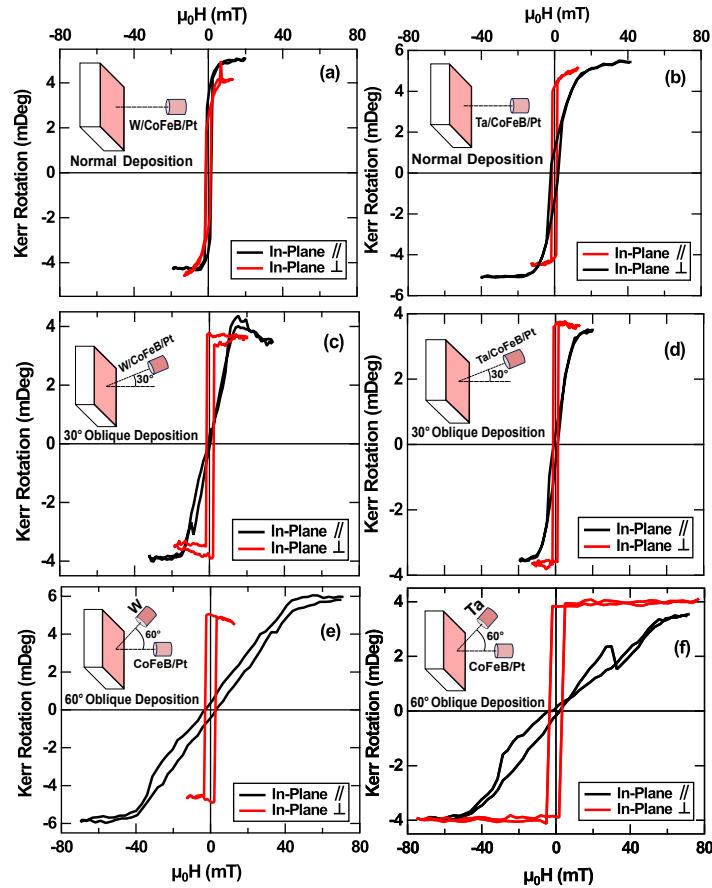


FIG. 2. L-MOKE hysteresis loops measurement with the external magnetic field  $H$  for normal & oblique deposition of NM (W or Ta) seed layer in NM/CoFeB/Pt structures. (a) & (b) NM at  $0^\circ$ , (c) & (d) NM at  $30^\circ$  and (e) & (f) NM at  $60^\circ$ .

Both the Ta and W underlayers give similar results for the UMA. A weak UMA in the  $\theta = 0^\circ$  samples was traced back to the substrate quality, where the substrates appear to have polishing traces (within their specified roughness) that induce the UMA independent of the sample alignment in the deposition system. This was not observed with higher-quality substrates, such as industrial-grade silicon wafers, which were used for control samples. We thus demonstrated that the UMA can be tuned by changing the incident flux angle of the NM underlayer and a larger UMA can be achieved. We utilized these high-anisotropy spintronic structures for field-free THz emission and present the results in the following.

Femtosecond laser pulses used in our THz emission experiments are generated by a Ti:Sapphire laser operating at a 1 kHz repetition rate with a pulse width of 100 fs centered at a wavelength of 800 nm. These pulses were split into pump and probe beams. The pump beam was chopped at 500 Hz. The stronger pump pulses with a fluence of  $0.40 \text{ mJ/cm}^2$  (if not stated otherwise) irradiated the sample at normal incidence. The THz emission generated by the excited structures were subsequently detected using electro-optic sampling (EOS)<sup>24</sup> with a  $500 \mu\text{m}$  ZnTe crystal detector. The THz emission spectra of the samples are presented in Fig. 3 (a) and (b). Here, an external magnetic field of 60 mT was applied in the plane of the spintronic structure which is enough to saturate the

magnetization of ferromagnetic layer and THz emission was recorded.

The results show that the THz emission amplitude from the  $W0^\circ$  sample is approximately 17% higher compared to the  $W30^\circ$  and  $W60^\circ$  samples. This might be due to the interface roughness introduced with the oblique deposition or due to slight variations of the W layer thickness at different  $\theta$ , which was not completely compensated with the variation of the deposition times. Previous studies have shown that the transmission of spin current from the FM layer to the non-magnetic layer depends critically on thickness and surface quality.<sup>25</sup> Furthermore, the external magnetic field was then removed to record the THz emission amplitude in field-free environment for the structures ( $W60^\circ$ ,  $Ta30^\circ$  and  $Ta60^\circ$ ). As shown in the Fig. 3 (c) and (d) the THz signal was stable with no significant reduction in THz amplitude at zero field. Experiments over one hour with multiple recorded THz waveforms showed no degradation of the emission amplitude over time without the external field (not shown).

The effect of the pump fluence on the THz field strength was investigated for samples  $W60^\circ$  and  $Ta60^\circ$  with and without an external magnetic field. As Fig. 4 shows, the THz amplitude increases with increasing pump fluence. The excited spin current depends on the electron temperature, which is expected to rise linearly with the pump fluence. Therefore, the

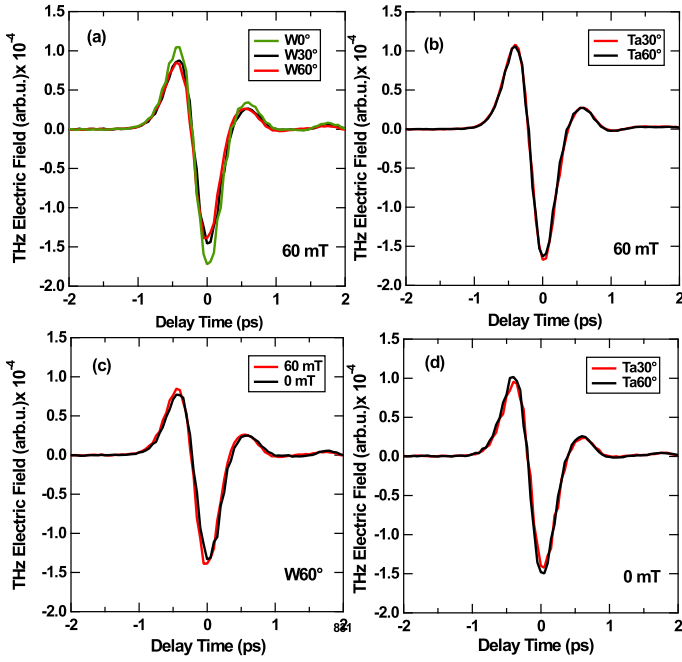


FIG. 3. THz signals from the oblique deposited NM (W or Ta) seed layer, in NM/CoFeB/Pt structures with and without the external magnetic field. (a) THz signal emitted from the samples  $W0^\circ$ ,  $W30^\circ$  and  $W60^\circ$  at 60 mT. (b) THz signal emitted from the samples  $Ta30^\circ$  and  $Ta60^\circ$  at 60 mT. (c) THz signal emitted from the sample  $W60^\circ$  at 0 & 60 mT. (d) THz signal emitted from the samples  $Ta30^\circ$  and  $Ta60^\circ$  at 0 mT.

simple expectation is a linear dependence of the THz amplitude on the pump fluence. However, a deviation from this linear behaviour is observed in our experiment (see straight lines in Fig. 4 (a) and (b)). This is due to the ultrafast demagnetization, only a given amount of spins is available for thermal extraction from the FM layer and leads to the observed saturation<sup>7,26</sup>. However, no decrease in the THz amplitude with increasing pump fluence up to  $\approx 1.4 \text{ mJ/cm}^2$  is observed, which is in agreement with the previous study<sup>21</sup>. Importantly, this indicates that there is no damage to the film structure. Also, no hysteresis was observed in the THz emission from the  $W60^\circ$  sample when subjected to varying pump fluence ( $\approx 0.37 - 1.4 \text{ mJ/cm}^2$ ) first at 60 mT and later at 0 mT, (see Fig. 4(a)). Here, it is also observed that  $Ta60^\circ$  generates 5 to 11% higher peak-to-peak THz amplitude than  $W60^\circ$  under the same pump fluence, which is contrary to the previous findings<sup>2</sup>.

The complex sheet conductance was measured using THz time domain spectroscopy (THz-TDS), and Drude model<sup>27</sup> fits of the real part were performed. The imaginary part is effectively zero within experimental error and is not shown in the sheet conductance plots. Drude model fits revealed short scattering times of  $\sim 1$  to 2 fs, in agreement with literature on scattering times in metallic thin films<sup>27</sup>. The  $W60^\circ$  have higher DC sheet conductance than  $Ta60^\circ$  (see Fig. 4 (c),(d)) and based on parallel resistivity model<sup>28</sup> with  $\rho_{Pt}(2 \text{ nm}) \approx 70 \mu\Omega \cdot \text{cm}$ <sup>29</sup> and  $\rho_{CFB}(2 \text{ nm}) \approx 180 \mu\Omega \cdot \text{cm}$  it is found that the W layer has lower resistivity ( $\approx 110 \mu\Omega \cdot \text{cm}$ ) than the bulk  $\beta$ -

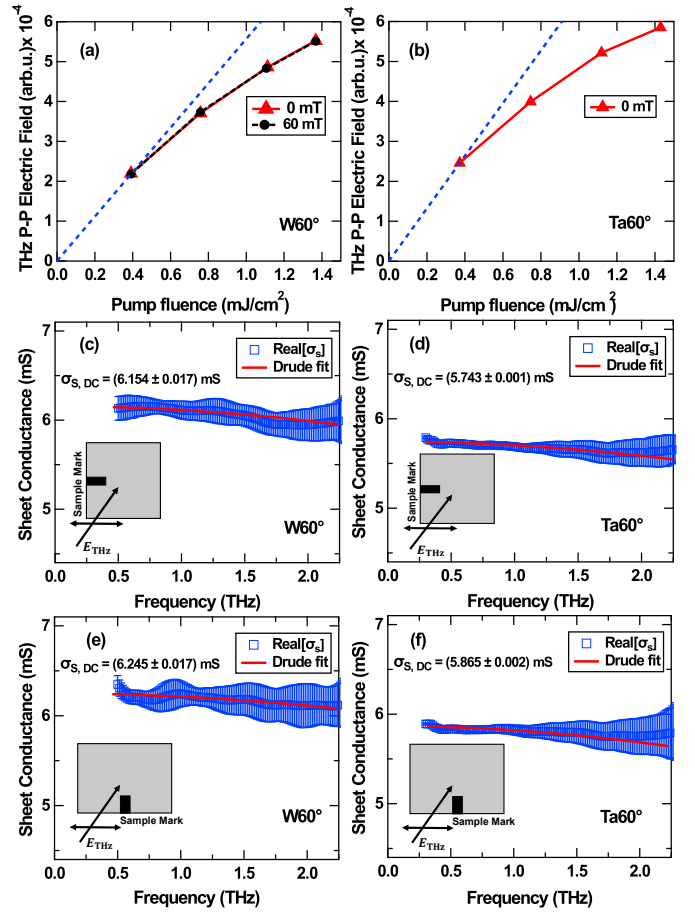


FIG. 4. THz emission as a function of pump fluence and a Drude model fit (red solid line) of the real part sheet conductance spectra at room temperature: THz peak-to-peak amplitude (a)  $W60^\circ$  at 60 & 0 mT, and (b)  $Ta60^\circ$  at 0 mT (blue dashed line acts as a guide for the eye), (c) & (e) sheet conductance spectra for  $W60^\circ$  and (d) & (f) sheet conductance spectra for  $Ta60^\circ$ . Inset: Sample orientation during THz-TDS for measurement of complex sheet conductance spectra, where sample mark represents ripple direction of obliquely deposited NM underlayer.

phase W resistivity (typically around  $200 \mu\Omega \cdot \text{cm}$ )<sup>30</sup>. While tungsten with high resistivity in the  $\beta$ -phase yields a high spin Hall angle<sup>31</sup> and strong THz signal, lower-resistivity W will likely result in lower THz emission amplitude, in agreement with our observation. We also observed that the sheet conductivity of both the sample  $W60^\circ$  and  $Ta60^\circ$  is anisotropic. Specifically, the sheet conductance is lower when  $E_{\text{THz}}$  field is perpendicular to the ripple direction (see Fig. 4(c),(d)) and higher when  $E_{\text{THz}}$  field is parallel to the ripple direction (see Fig. 4(e),(f)). When  $E_{\text{THz}}$  field is parallel to the ripples, charge carriers experience less scattering as compared to a charge flow transverse to the ripple direction. The observation of the sheet conductance anisotropy is direct evidence for the structural anisotropy in the samples. We note that this result can not be explained by anisotropic magnetoresistance, which would lead to a higher sheet conductance in the configuration with  $E_{\text{THz}}$  perpendicular to the ripple direction.

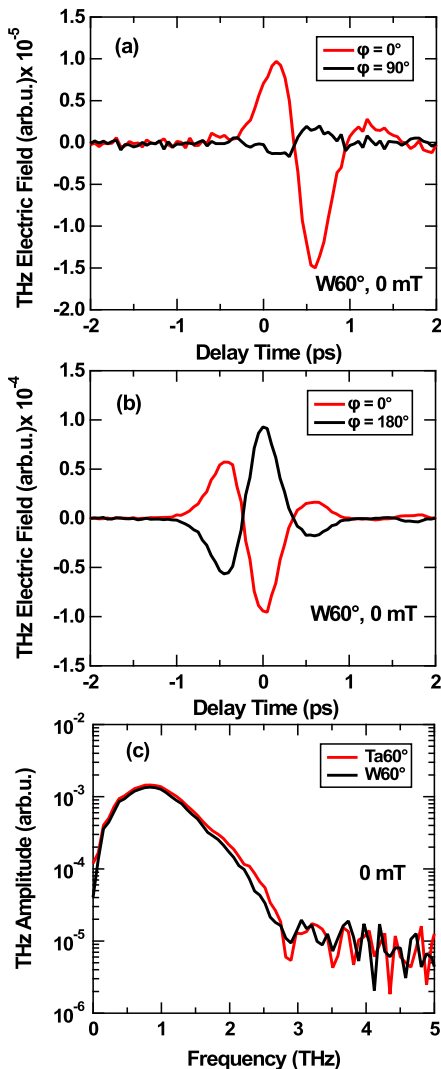


FIG. 5. The polarization state of the emitted THz waveform and corresponding THz amplitude spectra. (a) THz amplitude measured with polarizer at  $\varphi = 0^\circ$  and  $90^\circ$ . (b) THz emission at  $\varphi = 0^\circ$  and  $180^\circ$  (c) THz amplitude spectra by fast fourier transformation.

Furthermore, we expect that the THz pulses from the STEs exhibit linear polarization perpendicular to the in-plane magnetization direction<sup>2,25,32</sup>. To determine the polarization state, a polarizer was inserted between the STE and the ZnTe detector. The THz emission was then recorded for the sample W60° with  $\varphi = 0^\circ$ , and  $90^\circ$ , (where  $\varphi$  just refers to the rotation of the sample around the laser beam direction). This rotation resulted in a complete suppression of the THz signal, indicating a well-defined polarization direction for the emitted THz pulse, see Fig. 5 (a). The polarization of the STEs can be controlled by both the applied magnetic field and the azimuthal rotation of the spintronic structure about the surface normal. Phase control through azimuthal rotation in zero external magnetic field is demonstrated in Fig. 5(b) by rotating the sample  $180^\circ$  relative to its initial orientation. However, in presence of the external magnetic field THz emission is, as expected, invariant of azimuthal rotation. In the THz amplitude

spectra (Fig. 5(c)), the spectral width is limited by both the  $500\ \mu\text{m}$  thick ZnTe crystal detector and the 100 fs laser pulse duration used in this investigation. Shorter laser pulse durations and a relatively thinner ZnTe crystal detector could be used during the experiment for higher detected spectral bandwidth.

In summary, we have demonstrated in-plane uniaxial magnetic anisotropy in the ferromagnetic layer by utilizing an obliquely deposited non-magnetic underlayer in trilayer spintronic THz emitter structures. Notably, all structures exhibited anisotropies with the easy axis perpendicular to the ripple direction. The spintronic structures with high anisotropies were successfully employed to generate terahertz emission without the need for an external magnetic field. The emitted THz radiation exhibits linear polarization, and its polarization can be controlled by both varying the direction of an applied external magnetic field (when present) and by the azimuthal rotation of the sample in the absence of an external magnetic field. Operating spintronic THz emitters in a field-free environment not only eliminates a disadvantage with respect to electro-optic crystals and semiconductor antenna tabletop THz sources but also opens doors for integration, high-density multi-emitter systems, practical applications in communication, and security imaging<sup>33</sup>.

## ACKNOWLEDGMENT

The Darmstadt group acknowledges the financial support by the Deutsche Forschungsgemeinschaft under Project No. 513154775 and No. 518575758, and by the DFG Major Research Instrumentation programme Project No. 511340083 and Project No. 468939474. The group in Bielefeld acknowledges the financial support from the European Union's Horizon 2020 research and innovation program (Grant Agreement No.964735 EXTREME-IR), Deutsche Forschungsgemeinschaft (DFG) within Project No. 468501411-SPP2314 INTEGRATECH and Project No. 518575758 HIGHSPINTERA, Bundesministerium für Bildung und Forschung (BMBF) within Project No. 05K2022 PBA Tera-EXPOSE, and Bielefelder Nachwuchsfond. We, gratefully acknowledge Prof. Lambert Alff at Technical University Darmstadt for providing us with access to his laboratory's X-ray diffractometer, which was instrumental in carrying out this research work.

## AUTHOR DECLARATIONS

### Conflict of Interest

The authors have no conflicts to disclose.

## DATA AVAILABILITY

The data that support the findings of this study are available from the corresponding author upon reasonable request.



## REFERENCES

- <sup>1</sup>T. Kampfrath, M. Battiato, P. Maldonado, G. Eilers, J. Nötzold, S. Mährlein, V. Zbarsky, F. Freimuth, Y. Mokrousov, S. Blügel, M. Wolf, I. Radu, P. M. Oppeneer, and M. Münzenberg, "Terahertz spin current pulses controlled by magnetic heterostructures," *Nature Nanotechnology* **8**, 256 (2013).
- <sup>2</sup>T. Seifert, S. Jaiswal, U. Martens, J. Hannegan, L. Braun, P. Maldonado, F. Freimuth, A. Kronenberg, J. Henrizi, I. Radu, E. Beaurepaire, Y. Mokrousov, P. M. Oppeneer, M. Jourdan, G. Jakob, D. Turchinovich, L. M. Hayden, M. Wolf, M. Münzenberg, M. Kläui, and T. Kampfrath, "Efficient metallic spintronic emitters of ultrabroadband terahertz radiation," *Nature Photonics* **10**, 483 (2016).
- <sup>3</sup>H. Jiao and G. E. Bauer, "Spin backflow and ac voltage generation by spin pumping and the inverse spin hall effect," *Physical Review Letters* **110**, 217602 (2013).
- <sup>4</sup>J. Sinova, S. O. Valenzuela, J. Wunderlich, C. H. Back, and T. Jungwirth, "Spin hall effects," *Reviews of Modern Physics* **87**, 1213 (2015).
- <sup>5</sup>T. Seifert, S. Jaiswal, M. Sajadi, G. Jakob, S. Winnerl, M. Wolf, M. Kläui, and T. Kampfrath, "Ultrabroadband single-cycle terahertz pulses with peak fields of 300 kv cm<sup>-1</sup> from a metallic spintronic emitter," *Applied Physics Letters* **110**, 252402 (2017).
- <sup>6</sup>S. Kumar and S. Kumar, "Ultrafast terahertz spin and orbital transport in magnetic/nonmagnetic multilayer heterostructures and a perspective," *Journal of Applied Physics* **134**, 170901 (2023).
- <sup>7</sup>R. Rouzegar, L. Brandt, L. Nádvořík, D. A. Reiss, A. L. Chekhov, O. Gueckstock, C. In, M. Wolf, T. S. Seifert, P. W. Brouwer, G. Woltersdorf, and T. Kampfrath, "Laser-induced terahertz spin transport in magnetic nanostructures arises from the same force as ultrafast demagnetization," *Physical Review B* **106**, 144427 (2022).
- <sup>8</sup>D. Kong, X. Wu, B. Wang, T. Nie, M. Xiao, C. Pandey, Y. Gao, L. Wen, W. Zhao, C. Ruan, J. Miao, Y. Li, and L. Wang, "Broadband spintronic terahertz emitter with magnetic-field manipulated polarizations," *Advanced Optical Materials* **7**, 1900487 (2019).
- <sup>9</sup>M. T. Hibberd, D. S. Lake, N. A. Johansson, T. Thomson, S. P. Jamison, and D. M. Graham, "Magnetic-field tailoring of the terahertz polarization emitted from a spintronic source," *Applied Physics Letters* **114**, 031101 (2019).
- <sup>10</sup>Y. A. Wei, P. J. Wu, P. Y. Tsai, K. L. Chen, and C. S. Yang, "Enhanced tunable terahertz mie resonance and magnetoplasmonic effect through chain formation in ferrofluid," *Applied Physics Letters* **123**, 091101 (2023).
- <sup>11</sup>M. Shalaby, M. Peccianti, Y. Ozturk, M. Clerici, I. Al-Naib, L. Razzari, T. Ozaki, A. Mazhorova, M. Skorobogatiy, and R. Morandotti, "Terahertz faraday rotation in a magnetic liquid: High magneto-optical figure of merit and broadband operation in a ferrofluid," *Applied Physics Letters* **100**, 241107 (2012).
- <sup>12</sup>R. Schneider, M. Fix, R. Heming, S. M. D. Vasconcellos, M. Albrecht, and R. Bratschitsch, "Magnetic-field-dependent thz emission of spintronic tbfe/pt layers," *ACS Photonics* **5**, 3936 (2018).
- <sup>13</sup>S. M. Hewett, C. Bull, A. M. Shorrock, C. H. Lin, R. Ji, M. T. Hibberd, T. Thomson, P. W. Nutter, and D. M. Graham, "Spintronic terahertz emitters exploiting uniaxial magnetic anisotropy for field-free emission and polarization control," *Applied Physics Letters* **120**, 122401 (2022).
- <sup>14</sup>E. Kueny, A. L. Calendron, S. Velten, L. Bocklage, F. X. Kärtner, and R. Röhlberger, "Spin-structured multilayer thz emitters by oblique incidence deposition," *Journal of Applied Physics* **133**, 033903 (2023).
- <sup>15</sup>S. van Dijken, G. D. Santo, and B. Poelsema, "Influence of the deposition angle on the magnetic anisotropy in thin co films on cu(001)," *Physical Review B - Condensed Matter and Materials Physics* **63**, 10 (2001).
- <sup>16</sup>H. Ono, M. Ishida, M. Fujinaga, H. Shishido, and H. Inaba, "Texture, microstructure, and magnetic properties of fe-co alloy films formed by sputtering at an oblique angle of incidence," *Journal of Applied Physics* **74**, 5124 (1993).
- <sup>17</sup>S. Scheibler, O. Yildirim, I. K. Herrmann, and H. J. Hug, "Inducing in-plane uniaxial magnetic anisotropies in amorphous cofeb thin films," *Journal of Magnetism and Magnetic Materials* **585**, 171015 (2023).
- <sup>18</sup>Y. Fukuma, Z. Lu, H. Fujiwara, G. J. Mankey, W. H. Butler, and S. Matsumura, "Strong uniaxial magnetic anisotropy in cofe films on obliquely sputtered ru underlayer," *Journal of Applied Physics* **106**, 076101 (2009).
- <sup>19</sup>R. D. McMichael, C. G. Lee, J. E. Bonevich, P. J. Chen, W. Miller, and W. F. Egelhoff, "Strong anisotropy in thin magnetic films deposited on obliquely sputtered ta underlayers," *Journal of Applied Physics* **88**, 5296 (2000).
- <sup>20</sup>X. Wu, H. Wang, H. Liu, Y. Wang, X. Chen, P. Chen, P. Li, X. Han, J. Miao, H. Yu, C. Wan, J. Zhao, and S. Chen, "Antiferromagnetic-ferromagnetic heterostructure-based field-free terahertz emitters," *Advanced Materials* **34**, 2204373 (2022).
- <sup>21</sup>S. Liu, Z. Ren, P. Chen, S. Chen, M. Zhang, Z. Yang, D. Kong, J. Wang, Y. Li, J. Ma, X. Lu, B. Zhang, Z. Liu, X. Han, C. Wan, Y. Li, R. Singh, and X. Wu, "External-magnetic-field-free spintronic terahertz strong-field emitter," *Ultrafast Science* **4**, 0060 (2024).
- <sup>22</sup>A. Barranco, A. Borrás, A. R. Gonzalez-Elipe, and A. Palmero, "Perspectives on oblique angle deposition of thin films: From fundamentals to devices," *Progress in Materials Science* **76**, 59 (2016).
- <sup>23</sup>S. V. Dijken, L. C. Jorritsma, and B. Poelsema, "Steering-enhanced roughening during metal deposition at grazing incidence," *Physical review letters* **82**, 4038 (1999).
- <sup>24</sup>Q. Wu and X. C. Zhang, "Free-space electro-optic sampling of terahertz beams," *Applied Physics Letters* **67**, 3523 (1995).
- <sup>25</sup>G. Li, R. Medapalli, R. V. Mikhaylovskiy, F. E. Spada, T. Rasing, E. E. Fullerton, and A. V. Kimel, "Thz emission from co/pt bilayers with varied roughness, crystal structure, and interface intermixing," *Physical Review Materials* **3**, 084415 (2019).
- <sup>26</sup>J. Varela-Manjarres, A. Kefayati, M. B. Jungfleisch, J. Q. Xiao, and B. K. Nikolic, "Charge and spin current pumping by ultrafast demagnetization dynamics," **110**, L060410 (2024).
- <sup>27</sup>N. S. Beermann, S. Fabretti, H. A. Hafez, M. A. Syskaki, I. Kononenko, G. Jakob, M. Kläui, and D. Turchinovich, "Electronic transparency of internal interfaces in metallic nanostructures comprising light, heavy and ferromagnetic metals measured by terahertz spectroscopy," *Nanophotonics* **13**, 1883 (2024).
- <sup>28</sup>Y. Y. Chen and J. Y. Juang, "Finite element analysis and equivalent parallel-resistance model for conductive multilayer thin films," *Measurement Science and Technology* **27**, 074006 (2016).
- <sup>29</sup>M. H. Nguyen, D. C. Ralph, and R. A. Buhrman, "Spin torque study of the spin hall conductivity and spin diffusion length in platinum thin films with varying resistivity," *Physical Review Letters* **116**, 126601 (2016).
- <sup>30</sup>Q. Hao, W. Chen, and G. Xiao, "Beta ( $\beta$ ) tungsten thin films: Structure, electron transport, and giant spin hall effect," *Applied Physics Letters* **106**, 182403 (2015).
- <sup>31</sup>W. Chen, G. Xiao, Q. Zhang, and X. Zhang, "Temperature study of the giant spin hall effect in the bulk limit of  $\beta$ -w," *Physical Review B* **98**, 134411 (2018).
- <sup>32</sup>D. Khusyainov, S. Ovcharenko, M. Gaponov, A. Buryakov, A. Klimov, N. Tiercelin, P. Pernod, V. Nozdrin, E. Mishina, A. Sigov, and V. Preobrazhensky, "Polarization control of thz emission using spin-reorientation transition in spintronic heterostructure," *Scientific Reports* **11**, 697 (2021).
- <sup>33</sup>X. Li, J. Li, Y. Li, A. Ozcan, and M. Jarrahi, "High-throughput terahertz imaging: progress and challenges," *Light: Science & Applications* **12**, 233 (2023).